AGU PUBLICATIONS

JGR

Journal of Geophysical Research: Space Physics

RESEARCH ARTICLE
10.1002/2016JA023323

Key Points:
- Using Magnetospheric Multiscale (MMS) data, we were able to measure a small guide field near the magnetic reconnection X point
- That guide field was roughly about 2.5 nT, about 0.1 times the magnetosheath reconnection field, for the 16 October 2015 event at 1307 UT
- The component of magnetic field normal to the reconnection plane had approximate quadrupolar structure around the reconnection X point

Correspondence to:
R. E. Denton,
richard.e.denton@dartmouth.edu

Citation:
Denton, R. E., B.U. Ö. Sonnerup, H. Hasegawa, T. D. Phan, C. T. Russell, R. J. Strangeway, B. L. Giles, and R. B. Torbert (2016), Reconnection guide field and quadrupolar structure observed by MMS on 16 October 2015 at 1307 UT, *J. Geophys. Res. Space Physics*, *121*, 9880–9887, doi:10.1002/2016JA023323.

Received 12 AUG 2016
Accepted 4 OCT 2016
Accepted article online 7 OCT 2016
Published online 25 OCT 2016

Reconnection guide field and quadrupolar structure observed by MMS on 16 October 2015 at 1307 UT

R. E. Denton[1], B. U. Ö. Sonnerup[2], H. Hasegawa[3], T. D. Phan[4], C. T. Russell[5], R. J. Strangeway[5], B. L. Giles[6], and R. B. Torbert[7]

[1]Department of Physics and Astronomy, Dartmouth College, Hanover, New Hampshire, USA, [2]Thayer School of Engineering, Dartmouth College, Hanover, New Hampshire, USA, [3]Institute of Space and Astronautical Science, JAXA, Sagamihara, Japan, [4]Space Science Laboratory, University of California, Berkeley, California, USA, [5]Institute of Geophysics and Planetary Physics, University of California, Los Angeles, California, USA, [6]NASA Goddard Space Flight Center, Greenbelt, Maryland, USA, [7]Institute for the Study of Earth, Oceans, and Space, University of New Hampshire, Durham, New Hampshire, USA

Abstract We estimate the guide field near the X point, B_{M0}, for a magnetopause crossing by the Magnetospheric Multiscale (MMS) spacecraft at 1307 UT on 16 October 2015 that showed features of electron-scale reconnection. This component of the magnetic field is normal to the reconnection plane *L*-*N* containing the reconnection magnetic field, B_L, and the direction $\mathbf{e}_N$ normal to the current sheet. The B_M field component appears to approximately have quadrupolar structure close to the X point. Using several different methods to estimate values of the guide field near the X point, some of which use an assumed quadrupolar symmetry, we find values ranging between −3.1 nT and −1.2 nT, with a nominal value of about −2.5 nT. The rough consistency of these values is evidence that the quadrupolar structure exists.

1. Introduction

Burch et al. [2016] and *Torbert et al.* [2016] identified a magnetic reconnection event observed by NASA's Magnetospheric Multiscale (MMS) Mission on 16 October 2015 near 1307 UT that probed the electron diffusion region, that region where electron-scale kinetic processes control the electric field [*Hesse et al.*, 2014]. *Denton et al.* [2016] evaluated the motion of the MMS spacecraft through the reconnection structure. They showed that the structure of the "out-of-plane" magnetic field component, B_M, appeared to be quadrupolar. They also showed that the MMS 4 spacecraft approached nearest to the X point and that at that time MMS 4 observed a small negative value of B_M, ~ −2.5 nT.

In this paper, we present further evidence for the quadrupolar structure and guide field for this event. Preceding the magnetopause crossing that occurred near 1307 UT, there was a more complete crossing that occurred just before 1306 UT. Because the components of **B** perpendicular to the direction of the reconnection magnetic field were small and unsteady, it was not possible to estimate a guide field from these observations. Here we concentrate on estimating the guide field at the X point, B_{M0}, and we use a number of different techniques to evaluate this value.

A value of −2.5 nT is small compared to the asymptotic magnetosphere reconnection field of 39 nT northward and the asymptotic magnetosheath reconnection field of at least 23 nT southward [*Burch et al.*, 2016]. While the reconnection rate is not greatly affected by a small guide field [*Swisdak et al.*, 2005], some studies suggest that even this small a guide field could affect the structure of the electron diffusion region by changing the nature of the electron orbits close to the X point [*Karimabadi et al.*, 2005; *Goldman et al.*, 2011].

2. Background Information

Denton et al. [2016] studied the motion of the MMS spacecraft through the reconnection structure observed on 16 October 2015 at 1307 UT using fluxgate magnetometer data [*Russell et al.*, 2014] and ion and electron bulk velocity moments from the Fast Plasma Instrument (FPI) [*Pollock et al.*, 2016]. The data were downloaded at burst mode resolution, 7.8 ms for the magnetometer, 30 ms for the electron data, and 150 ms for the ion data. For most purposes, the magnetometer data were smoothed with a boxcar average to a final resolution of 39 ms.

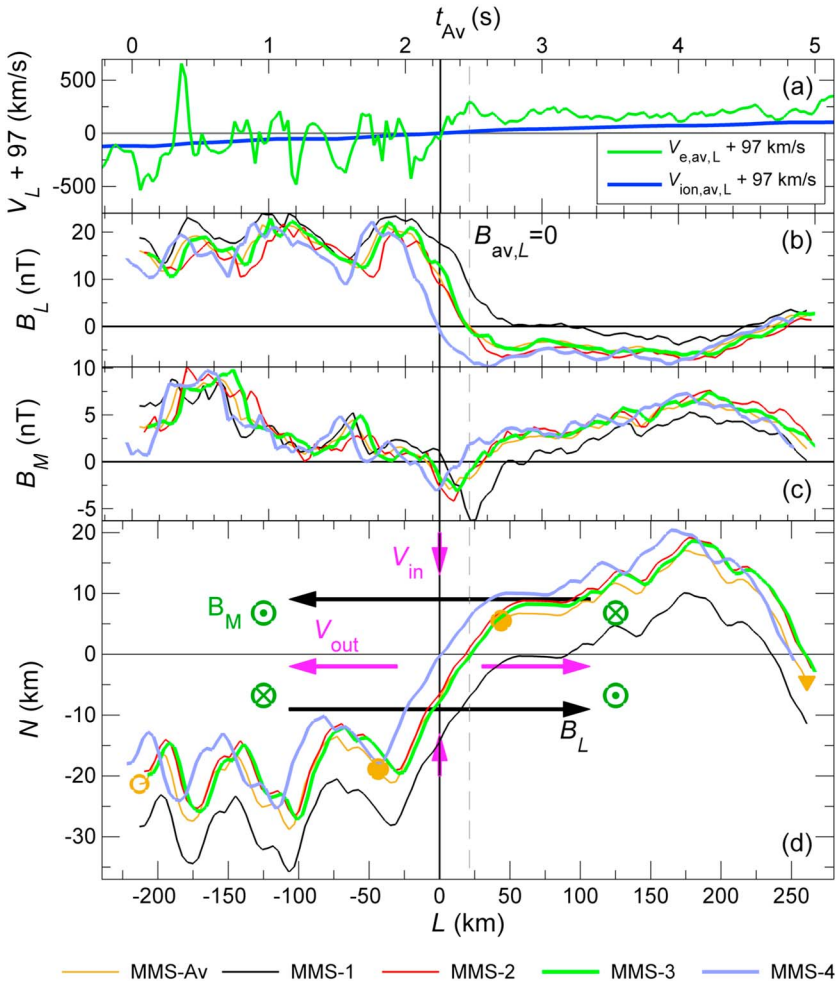

Figure 1. Spacecraft paths: (d) Trajectory of MMS centroid (MMS-Av) and of individual MMS spacecraft relative to the reconnection structure in the *L*-*N* plane with the X point at the origin. The centroid started at the open gold circle and ended at the downward pointing gold triangle. The gold curve is especially reliable between the gold-filled circles. (b, c) The B_L and B_M (positive into the page) versus t_{Av} at the top of the plot; t_{Av} is the real time (following 1307 UT) only for MMS-Av. The other curves have been shifted so that the observed field components line up vertically with the corresponding position in Figure 1d. (a) The average *L* component of the electron (green) and ion (blue) velocities shifted up by 97 km/s. The solid black and dashed gray vertical lines are respectively at $L=0$ (average shifted flow velocity reversal) and at the magnetic reversal (where B_L for MMS-Av is zero). In GSM, $\mathbf{e}_L=(0.311,0.488,0.816)$, $\mathbf{e}_M=(0.480,-0.820,0.307)$, and $\mathbf{e}_N=(0.819, 0.296, -0.490)$. (Adapted from Figures 4 and 2 of *Denton et al.* [2016])

First, *Denton et al.* [2016] defined an *LMN* coordinate system with $\mathbf{e}_L=(0.311, 0.488, 0.816)$ in geocentric solar magnetospheric (GSM) coordinates along the reconnection magnetic field, roughly northward; with $\mathbf{e}_N=(0.819, 0.296, -0.490)$ across the current sheet, roughly outward; and with $\mathbf{e}_M=(0.480, -0.820, 0.307)$, roughly westward. For the *L* direction, they used the direction of maximum variance of the magnetic field [*Sonnerup and Scheible*, 1998]. For the *N* direction, they used the maximum gradient direction from minimum directional derivative (MDD) analysis [*Shi et al.*, 2005], albeit, with a 2.7° correction to make it precisely perpendicular to $\mathbf{e}_L$. The maximum eigenvalues for both methods were well separated from the intermediate eigenvalues, indicating an excellent determination of these directions [*Denton et al.*, 2016].

To get the *N* component of the velocity of the magnetic structure relative to the spacecraft, *Denton et al.* [2016] used spatiotemporal difference (STD) analysis [*Shi et al.*, 2006]. Basically, the equation $d\mathbf{B}/dt=-\mathbf{V}_{str}\cdot\nabla\mathbf{B}$ was solved at each time for the structure velocity $\mathbf{V}_{str}$, using $\nabla\mathbf{B}$ from the MDD analysis and $d\mathbf{B}/dt$ from the time variation of the magnetic field *B* observed by MMS. The *L* and *M* components were not well determined by STD. Because we are seeking to find the motion in the *L*-*N* plane, the *M* component of $\mathbf{V}_{str}$ is not needed. The *L* component of the velocity was inferred from the plasma velocity. *Denton et al.* [2016]

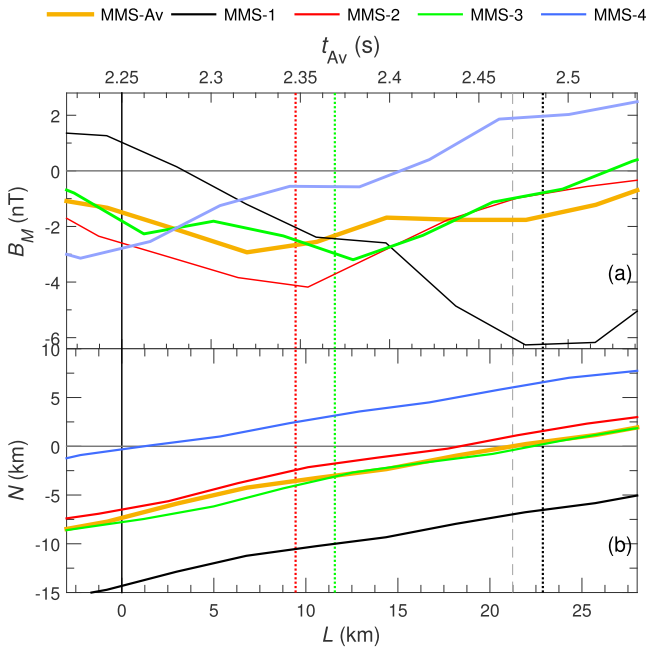

Figure 2. Expanded spacecraft paths: Similar to Figure 1 except that Figure 2b now shows the spacecraft paths only for the region close to the X point, and only B_M is shown in Figure 2a. The red, green, and black dotted vertical lines are drawn at L values where MMS 4 (blue curve in Figure 2b) is at a distance above the $N=0$ line equal to the distance that the other spacecraft (MMS 2, 3, and 1 for red, green, and black, respectively) is below the $N=0$ line.

found that the L components of both the ion and electron velocities reversed and increased linearly from a point where their common velocity was −97 km/s (Figure 1a), so they assumed that this was the velocity of the magnetic structure.

By integrating the velocities described above, *Denton et al.* [2016] found the motion of the MMS spacecraft in the reconnection plane (the plane containing L and N) with the projected trajectories shown in Figure 1d. They defined the position of the X point (the origin in Figure 1d) using the value of the N coordinate where the reconnection magnetic field (the L component) reversed and the value of the L coordinate where the plasma flow (the L component) reversed. In Figure 1d, the black arrows, short magenta arrows, and long magenta arrows show respectively the directions of the reconnection magnetic field B_L, the plasma inflow velocity V_{in}, and the plasma outflow velocity V_{out}. (The velocity stagnation point is shown shifted in the N direction toward the magnetosphere side of the X point [*Cassak and Shay*, 2007], though our method does not yield the amount of the shift.) The green arrowheads into and out of the page show the expected directions of the Hall magnetic field for symmetric antiparallel reconnection (conditions which are not necessarily applicable for this event).

The thick gold curve in Figure 1d is the trajectory of the centroid of the MMS spacecraft ("MMS-Av") relative to the magnetic structure in the L-N plane. *Denton et al.* [2016] were most confident about the motion between $t=1.8$ s and 2.7 s, marked by the gold-filled circles on the thick gold curve in Figure 1d, because within that time range the results of the analysis did not vary as the method was altered. Figure 1d also shows the trajectories of the individual MMS spacecraft using the colors indicated in the legend at the bottom of the figure. These trajectories are displaced from the centroid trajectory by the relative displacement of each spacecraft. Figures 1b and 1c show B_L and B_M, respectively, averaged over the four spacecraft (MMS-Av) and for the individual spacecraft versus the time t_{Av}. This time is equivalent to t only for MMS-Av. The other curves have been shifted horizontally so that the observed field components line up vertically with the corresponding positions in Figure 1d. (See the starting points of the curves, which all correspond to the same initial time.)

Denton et al. [2016] emphasized that in reality there was some structure in the M direction. Because of this, the position of the X point in Figure 1d is most accurate in an average sense since it was found from the reversal of the magnetic field and plasma velocities averaged over the four spacecraft.

3. Estimates of the Guide Field Near the X Point

Figure 1d shows that MMS 4 (blue curve) came closest to the X point (the origin of Figure 1d). See also Figure 2, which shows the position and B_M for the spacecraft like in Figure 1 but for a smaller portion of the motion close to the X point.

Figure 3 shows the time-dependent magnetic field components observed by MMS 4 in more detail. The vertical gray line in Figure 3 marked "closest" is drawn at the time where MMS 4 was closest to the X point, with the position of that point determined using the data from all four spacecraft. Very close to this time, MMS

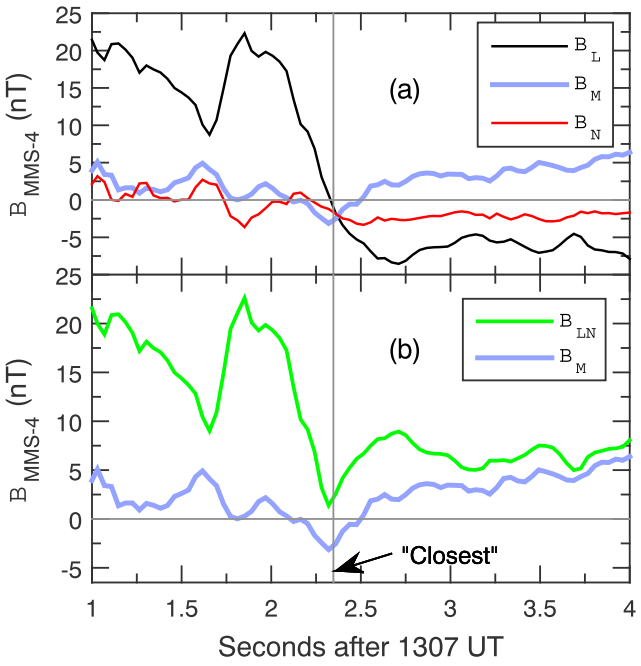

Figure 3. (a) Components of **B** observed by MMS 4 and (b) magnitude of the vector formed from the *L* and *N* components, B_{LN} and B_M, versus time. The vertical gray line marked closest is drawn at the time where MMS 4 was closest to the X point using the position of the X point determined using the data from all four spacecraft.

4 observed a sharp dip in the magnetic field in the reconnection (*L*-*N*) plane, $B_{LN}=\sqrt{B_L^2+B_N^2}$ (green curve in Figure 3b). At the time of the vertical gray line, B_M was −2.7 nT. This value is listed as estimate #1 for the guide field B_{M0} in the first row of Table 1.

The fact that the minimum in B_{LN} occurs slightly to the left of the vertical gray line in Figure 3b suggests that MMS 4 might have been closest to the X point slightly earlier than the analysis based on all four spacecraft would suggest, perhaps due to time dependence or structure in the *M* direction. Note that this minimum B_M is colocated with a minimum in B_{LN}. The minimum B_M observed by MMS 4 is −3.1 nT, listed as estimate #2 for B_{M0} in Table 1.

Figures 1d and 1c together suggest that B_M has a quadrupolar part. Note first the symmetrical pattern of B_M when the spacecraft are in the lower left quadrant of the *L*-*N* plane, compared to when they are in the upper right quadrant. When the spacecraft penetrate into the lower right quadrant, B_M becomes more negative. This is especially clear for MMS 1 (black curve in Figure 1) which penetrates most deeply into the lower right quadrant. Note also how much more positive B_M is for MMS 4 (blue curve in Figure 1) than for MMS 1, when MMS 4 is in the upper right quadrant and MMS 1 is in the lower right quadrant. Note finally that MMS 4 passes almost directly from the lower left *LN* quadrant to the upper right *LN* quadrant (Figure 1d) and that Figure 3b shows that B_M is roughly symmetric as MMS 4 passes by the X point (at the minimum of B_{LN}). This quadrupolar structure is not necessarily expected for asymmetric reconnection [*Mozer et al.*, 2008], and it was not prominent in a particle in cell simulation designed to simulate this event (M. Swisdak, private communication, 2016).

We will now assume a quadrupolar dependence for B_M of the form

$$B_M = B_{M0} + C_{BM} L N, \tag{1}$$

where C_{BM} is a constant, in order to find additional estimates of the guide field, B_{M0}, at the X point. The rough consistency of these estimates will be evidence that something like the quadrupolar symmetry of (1) does exist.

Table 1. Estimates of the Guide Field, B_{M0}

Estimate	Spacecraft Used	Method	B_{M0} (nT)
1	MMS 4	Closest (to X point from all spacecraft)	−2.7
2	MMS 4	Closest (to X point based on MMS 4 alone)	−3.1
3	MMS 4	Average at $N=0$ and $L=0$	−2.7
4	MMS-Av	Average at $N=0$ and $L=0$	−1.6
5	All	Average at $N=0$ and $L=0$	−1.6
6	MMS 4 with MMS 2	Average above and below $N=0$	−2.3
7	MMS 4 with MMS 3	Average above and below $N=0$	−1.7
8	MMS 4 with MMS 1	Average above and below $N=0$	−2.0
9	All	Eureqa fits	−3.1 nT to −1.2 nT

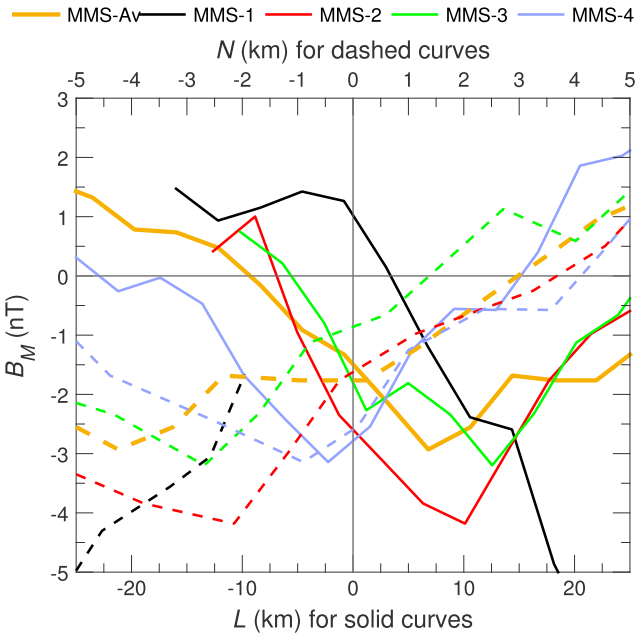

Figure 4. B_M versus L or N: (solid curves) B_M versus L on the bottom horizontal axis and (dashed curves) B_M versus N on the top horizontal axis. Curves are for the average data (MMS-Av) and individual spacecraft as indicated by the colors in the legend.

As suggested by (1), we first assume that B_M does not vary along the L axis (where $N = 0$) or the N axis (where $L = 0$). When MMS 4 crossed the N axis, $B_M = -2.8$ nT, and when MMS 4 crossed the L axis, $B_M = -2.6$ nT (Figure 2). Taking the average, we get −2.7 nT, which is estimate #3 for B_{M0} in Table 1. Since MMS 4 came very close to the X point (Figure 2b), this value is very close to estimates #1 and #2.

For an estimate based on the average spacecraft data, we can use the gold curves in Figures 2a and 2b. At the crossing of the N axis in Figure 2b, $B_{Av,M} = -1.5$ nT (Figure 2a), and at the crossing of the L axis, $B_{Av,M} = -1.8$ nT. The average of these values (using more significant digits before averaging) is −1.6 nT, entered as estimate #4 in Table 1.

Figure 4 shows how B_M varies for each of the spacecraft at the crossings of the N and L axes, using only the data between the gold-filled circles in Figure 1d. With the single exception of the crossing of the N axis by MMS 1 (black solid curve in Figure 4), all the B_M values are negative at $L = 0$ (solid curves) or $N = 0$ (dashed curves). Averaging the values for the individual spacecraft (other than gold curves) at all these crossings, including the solid black curve, we get $B_M = -1.6$ nT, listed as estimate #5 in Table 1. This is an independent estimate from that using the gold curves. In one case we have used the average B_M for the average trajectory, and in the other case, we have averaged the B_M for the separate crossings by the individual spacecraft.

Next we make use of the antisymmetry across the L axis, as suggested by Figure 1 and equation (1). In Figure 2b, the red, green, and black dotted vertical lines are locations where MMS 2 (red curve), MMS 3 (green curve), and MMS 1 (black curve) are located a distance below $N = 0$ equal to the distance that MMS 4 (blue curve) is above $N = 0$. For instance, at $L = 9.44$ km in Figure 2b, the blue curve is at $N = +2.48$ km, while the red curve is at $N = -2.48$ km. Averaging B_M for MMS 4 with that of the other spacecraft, we eliminate the antisymmetric component of B_M to get estimates of the guide field of −2.3 nT, −1.7 nT, and −2.0 nT, using MMS 2, 3, and 1, respectively. These values are listed as estimates #6–8 in Table 1.

Finally, we made use of the Eureqa nonlinear genetic regression software [*Schmidt and Lipson*, 2009] to find potential mathematical models for B_M, minimizing the squared deviation from the observed values in Figure 2. Each data point was equally weighted. Eureqa gives a family of "recommended solutions" of varying complexity. For each level of complexity, it gives the formula that best fits the data. The input variables that we used were L, N, and LN. Common mathematical operations plus exponentials, Gaussians, logarithms, and hyperbolic tangents were allowed in potential formulas. Division was excluded, because it led to unrealistic singularities in regions of the L-N plane that were not sampled. The quality of the resulting fits can be compared to that of a model using just a constant value equal to the average of B_M, −0.23 nT. For this simplest model, the mean square error is 3.7 nT^2.

A fit of the same mathematical form as (1) appeared in the family of solutions as

$$B_M = [-1.2 - 0.0044LN] \text{ nT}, \tag{2}$$

where L and N are measured in kilometers. The statistical R^2 value for this fit was 0.40, meaning that the formula "explained" 40% of the error or equivalently that the mean square error was reduced to 60% of that resulting from the fit to a constant value (−0.23 nT). That is, the mean square error using (2) was 0.60×3.7 nT$^2 = 2.2$ nT^2.

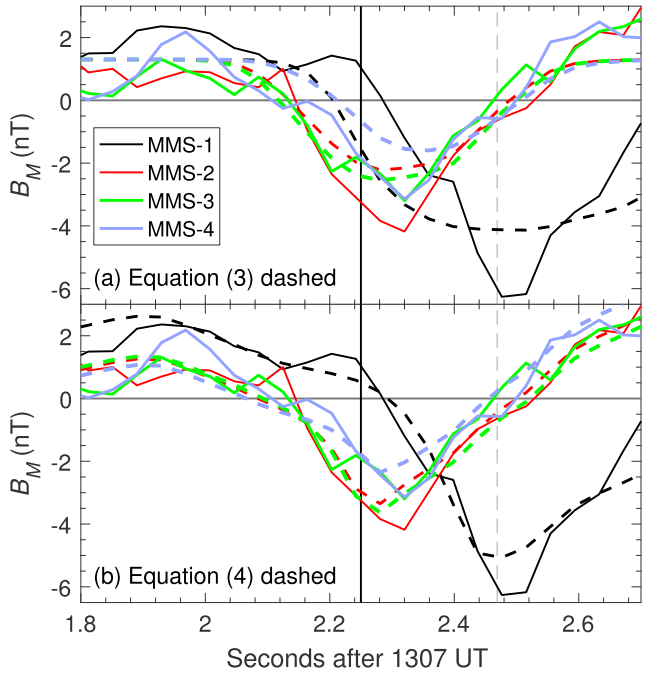

Figure 5. The solid curves are B_M observed by the individual spacecraft versus time. (a) The dashed curves show B_M predicted by (3) using the time-dependent L and N coordinates of the spacecraft. (b) The dashed curves show B_M predicted by (4).

The best fit involving only one of L, N, or L N was

$$B_M = [-1.6 + 2.9 \tanh(0.0090LN)] \text{ nT}, \tag{3}$$

with $R^2 = 0.78$ (0.8 nT^2 mean square error). This formula still has the same symmetry properties as (1).

More complicated recommended solutions did not have the same symmetries as (1). For instance the solution most highly recommended by Eureqa was

$$B_M = [-1.6 + 0.20N + 0.35N \tanh(1.6 + 0.31N + 0.088L)] \text{ nT}, \tag{4}$$

with $R^2 = 0.90$ (0.4 nT^2 mean square error). Equation (4) does not precisely support the symmetry of (1). It does lead to a tilted quadrupolar structure in B_M around $(L, N) = (-18, 0)$ km. But the asymptotic behavior of (1) at large N is probably not realistic. One should keep in mind that the spacecraft trajectories between the gold-filled circles in Figure 1 sample a very limited region of the L-N plane. Consequently, the fits may not be well constrained, and more complicated formulas such as (4) may not be accurate in regions of the L-N plane that were not sampled. Nevertheless, (4) does show that the quadrupolar symmetry is not exact, as is also suggested by the variation in guide field estimates in Table 1.

Figure 5 shows the time-dependent values of B_M observed by the spacecraft (solid curves) with the values resulting from (3) (dashed curves in Figure 5a) and (4) (dashed curves in Figure 5b). While (4) does lead to a better fit (comparing Figures 5a and 5b), (3) captures the main trends evident in the data.

Equations (3) and (4) give yet another estimate of the guide field at $L = N = 0$, namely, $B_{M0} = -1.6$ nT. Other recommended solutions yielded values of the guide field between −3.1 nT and −1.2 nT. This range is listed as estimate #9 in Table 1. Obviously, this is a very large range that does not narrow down the value very much, but this analysis does show that all the solutions yield a negative guide field.

4. Summary

We have shown how we can use the spacecraft trajectory calculated from the magnetic field and plasma velocities [*Denton et al.*, 2016] along with the observed symmetry properties of the out-of-plane magnetic

field to find estimates for the guide field near the X point, B_{M0}. Our estimates in Table 1 range from −1.2 nT to −3.1 nT. At the closest approach of MMS 4 to the X point, B_{M0} was either −2.7 nT (estimate #1, using the X point based on data from all the spacecraft) or −3.1 nT (estimate #2 at the minimum in B_{LN}; see Figure 3b). Using estimates based on the assumed quadrupolar symmetry (estimates #3–8), we find values for B_{M0} ranging between −1.6 nT and −2.7 nT, with a median value of −1.9 nT and a mean value of −2.0 nT. The values of B_{M0} from the recommended solutions of Eureqa ranged between −1.2 nT and −3.1 nT, with a median of −1.8 nT and a mean value of −2.1 nT. The solutions with many terms yielded B_{M0} close to −3.1 nT, the value from MMS 4 at minimum B_{LN}, while the simpler solutions (like (2)) yielded values closer to zero.

On the one hand, the −3.1 nT value might seem to be the best estimate for B_{M0} seeing as MMS 4 came closest to the X point. On the other hand, we know that there are variations between spacecraft, perhaps due to structure in the *M* direction, so we might prefer a value based on all the spacecraft data. Given the variation and the approximations involved, we cannot be certain about the exact number, but a guide field somewhere between −2 nT and −3 nT seems appropriate for this event. Thus, *Denton et al.*'s [2016] estimate of ∼ −2.5 nT seems reasonable.

Our assumption that the structure of B_M was approximately quadrupolar was based on the observations of B_M by the different MMS spacecraft as they traversed the different quadrants of the reconnection structure (Figure 1). The rough consistency of the estimates of the guide field near the X point based on this assumption demonstrates this symmetry.

But why did a simulation of this event not yield the quadrupolar structure (M. Swisdak, private communication, 2016)? Possibly, our analysis of the spacecraft motion is incorrect. But the *N* motion near the X point was very well determined from the magnetic data, and the *L* velocity of the structure could not have varied greatly or the relative ion velocity would not have appeared to vary so linearly (Figure 1a). Another possibility is that the observations were strongly affected by structure in the *M* direction. Another issue is that the asymptotic magnetosheath field was probably greater than the 23 nT assumed by *Burch et al.* [2016], since significant gradients in **B** continued to be observed on the magnetosheath side of the X point (not shown). Another issue is that particle in cell simulations typically assume an unrealistic mass ratio that may not lead to an accurate separation of electron and ion spatial scales. And another issue is that the simulation of this event did not include the inhomogeneity along the magnetic field from the magnetic equator toward the ionosphere or the effect of shear flow.

We have shown how a guide field at the X point, B_{M0}, can be determined, even when it is small. We are not claiming that quadrupolar structure is present for all reconnection events; further studies of MMS magnetopause crossings may clarify whether this event is typical or atypical.

Acknowledgments
Work at Dartmouth was supported by NASA grant NNX14AC38G. H.H. was supported by JSPS Grant-in-Aid for Scientific Research KAKENHI15K05306. We thank Marc Swisdak and Phil Pritchett for helpful conversations. B.G. thanks Dan Gershman, Levon Avanov, and John Dorelli for help in advancing the quality of the FPI products. MMS data are available at https://lasp.colorado.edu/mms/sdc/public/links. See also the supporting information of *Denton et al.* [2016].

References

Burch, J. L., et al. (2016), Electron-scale measurements of magnetic reconnection in space, *Science*, *352*(6290), aaf2939, doi:10.1126/science.aaf2939.

Cassak, P. A., and M. A. Shay (2007), Scaling of asymmetric magnetic reconnection: General theory and collisional simulations, *Phys. Plasmas*, *14*, 102114.

Denton, R. E., B. Sonnerup, H. Hasegawa, T. D. Phan, C. T. Russell, R. J. Strangeway, B. L. Giles, D. Gershman, and R. B. Torbert (2016), Motion of the MMS spacecraft relative to the magnetic reconnection structure observed on 16 Oct 2015 at 1307 UT, *Geophys. Res. Lett.*, *43*, 5589–5596, doi:10.1002/2016GL069214.

Goldman, M. V., G. Lapenta, D. L. Newman, S. Markidis, and H. Che (2011), Jet deflection by very weak guide fields during magnetic reconnection, *Phys. Rev. Lett.*, *107*(13), 135001, doi:10.1103/PhysRevLett.107.135001.

Hesse, M., N. Aunai, J. Birn, P. Cassak, R. E. Denton, J. F. Drake, T. Gombosi, M. Hoshino, W. Matthaeus, D. Sibeck, and S. Zenitani (2014), Theory and modeling for the Magnetospheric Multiscale Mission, *Space Sci. Rev.*, *199*, 577–630, doi:10.1007/s11214-014-0078-y.

Karimabadi, H., W. Daughton, and K. B. Quest (2005), Antiparallel versus component merging at the magnetopause: Current bifurcation and intermittent reconnection, *J. Geophys. Res.*, *110*, A03213, doi:10.1029/2004JA010750.

Mozer, F. S., P. L. Pritchett, J. Bonnell, D. Sundkvist, and M. T. Chang (2008), Observations and simulations of asymmetric magnetic field reconnection, *J. Geophys. Res.*, *113*, A00C03, doi:10.1029/2008JA013535.

Pollock, C., et al. (2016), Fast plasma investigation for magnetospheric multiscale, *Space Sci. Rev.*, *199*, 331–406, doi:10.1007/s11214-016-0245-4.

Russell, C. T., et al. (2014), The magnetospheric multiscale magnetometers, *Space Sci. Rev.*, *199*, 189–256, doi:10.1007/s11214-014-0057-3.

Schmidt, M., and H. Lipson (2009), Distilling free-form natural laws from experimental data, *Science*, *324*(5923), 81–85, doi:10.1126/science.1165893.

Shi, Q. Q., C. Shen, Z. Y. Pu, M. W. Dunlop, Q. G. Zong, H. Zhang, C. J. Xiao, Z. X. Liu, and A. Balogh (2005), Dimensional analysis of observed structures using multipoint magnetic field measurements: Application to Cluster, *Geophys. Res. Lett.*, *32*, L12105, doi:10.1029/2005GL022454.

Shi, Q. Q., C. Shen, M. W. Dunlop, Z. Y. Pu, Q. G. Zong, Z. X. Liu, E. Lucek, and A. Balogh (2006), Motion of observed structures calculated from multi-point magnetic field measurements: Application to Cluster, *Geophys. Res. Lett.*, *33*, L08109, doi:10.1029/2005GL025073.

Sonnerup, B., and M. Scheible (1998), Minimum and maximum variance analysis, in *Analysis Methods for Multi-Spacecraft Data*, edited by G. Paschmann, and P. Daly, pp. 185–220, Int. Space Sci. Inst., SR-001, Bern, Switzerland.

Swisdak, M., J. F. Drake, M. A. Shay, and J. G. McIlhargey (2005), Transition from antiparallel to component magnetic reconnection, *J. Geophys. Res.*, *110*, A05210, doi:10.1029/2004JA010748.

Torbert, R. B., et al. (2016), Estimates of the terms in Ohm's law during an encounter with an electron diffusion region, *Geophys. Res. Lett.*, *43*, 5918–5925, doi:10.1002/2016GL069553.